Practical Course M

Solid State: Electron Spin Resonance

Experiment performed on 11-12-2018

Alla Bezvershenko (7348847), Willem van der Feltz (7349034)
Supervisor: Anuja Sahasrabudhe

March 25, 2019

Contents

1 Introduction

This experiment is intended to study ESR measuring methods and applying them to learn about the structure of $CuSO_4{\cdot}5H_2O$. To do so, the material will be analysed both in single crystal and in powder form.

More can be learned about the energy level splitting (Zeeman effect) of the crystal by probing for resonance conditions where these levels are excited. By measuring the absorbance at different angles, information about the Landé tensor (g-tensor) can be retrieved which in turn provides information about the structure of the crystal. The broadness and shape of the resonance curves could give information about the spin-spin interactions inside the crystal.

2 Theoretical background

2.1 Electric structure of atoms

The electronic structure can be fundamentally deduced from the Schrödinger equation. The equation for the most simple molecule, hydrogen, looks as follows:

$$\Big(-\frac{\hbar^2}{2\mu}\nabla^2 - \frac{e^2}{4\pi\epsilon_0 r}\Big)\psi(r,\theta,\phi) = E\psi(r,\theta,\phi)$$

where μ is the reduced mass $\frac{m_e M}{m_e+M}$. Using the spherical symmetry it can be solved exactly. The result is a complicated function consisting of spherical harmonics and Laguerre polynomials.

Every result can be characterised by several so called quantum numbers: $\psi_{nlm}(r,\theta,\phi) := |n,l,m_l\rangle$. Quantum number $n = 1,2,3,...$ is called the principle quantum number and is related to the total energy. The quantum number $l = 0,1,2,...,n-1$ determines the total angular momentum. The so called magnetic number $m_l = -l,...,+l$ is related to its projection on the z-axis by

$$L_z = \hbar m_l.$$

For hydrogen, the energy eigenvalues are degenerate for l and m. In heavier, more complicated atoms, the degeneracy of l is broken due to shielding and spin-orbit coupling. The degeneracy of m is broken in a magnetic field, which is called the Zeeman effect. [1]

Another quantum number can be added: spin, s. For electrons it always has value 1/2. Its projection quantum number m_s can be in the range $-s,...,+s$ which means +1/2 or -1/2 for the electron. The total angular momentum can be introduced: $j = l + s$ and the eigenstates can be expressed as

$$|n,j,m_j,s,m_s\rangle$$

where $|l-s| \leq j \leq l+s$ and $m_j = -j,...+j$.

When considering more complicated systems with more electrons, these quantum numbers can still be used. As an approximation and using the Pauli exclusion principle, there can be only one particle per state and so with more electrons, the states are filled one by one. They are filled in order of increasing energy: the **Aufbau principle**. The states corresponding to a specific n are called a **shell**. Filled shells contribute zero total angular momentum ($J = 0$) and zero spin ($S = 0$). The order in which the shells get filled to minimize energy are dictated by Hund's rules [2]:

1. The total spin $S = \sum_i s_i$ has to be maximized.
2. The total angular momentum $L = \sum_i l_i$ has to be maximized.
3. If the outermost (highest n) shell is half-filled or less, the energy is minimized for the minimal total angular momentum $J = |L - S|$. If it is more than half filled, the energy is minimized for maximal total angular momentum $J = L + S$.

The electron configurations can be expressed in so called spectroscopic notation. Every l has its own name: $l = 0,1,2,3,4,5$ are called s,p,d,f,g,h respectively. E.g., a state with $n = 4, l = 3$ is

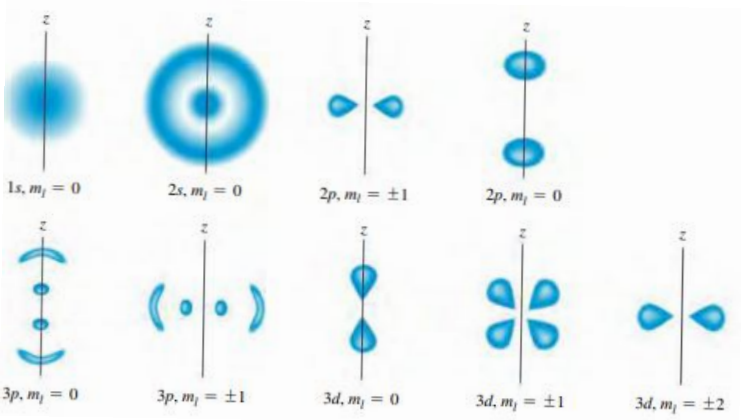

Figure 1: Cross sections of a few of the three dimensional orbitals of the hydrogen atom. [1]

denoted as $4f$. The amount of electrons actually in a certain shell is denoted with superscript. As an example, the electronic structure of carbon is $1s^2 2s^2 2p^2$.

The element relevant to this experiment is Cu^{2+}. The electronic configurations for Cu and Cu^{2+} are as follows:

$$Cu : [Ar]3d^{10}4s^1 \qquad Cu^{2+} : [Ar]3d^9. \tag{1}$$

We see that the relevant orbitals in Cu^{2+} are the d-orbitals. They correspond to the orbitals with $l = 2$ and there are five varieties for the different $m_l \in \{-2, -1, 0, 1, 2\}$. They are sketched in figure 2.

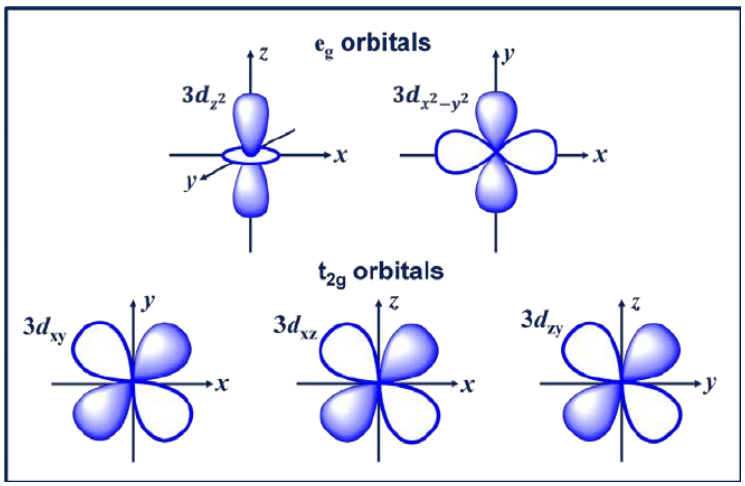

Figure 2: The different d-orbitals, subdivided into two classes, e_g and t_{2g}. [3]

2.2 Zeeman effect

The degeneracy in magnetic quantum number m_l is broken in a magnetic field. This is called the Zeeman effect and was discovered by Pieter Zeeman in 1896.

The effect can be explained as follows [1]: a plane current loop with vector area $\vec{A}$ and current I has magnetic moment $\vec{\mu}$ given by:

$$\vec{\mu} = I\vec{A}.$$

This magnetic moment can interact with a magnetic field $\vec{B}$ which generates potential energy U:

$$U = -\vec{\mu} \cdot \vec{B}. \tag{2}$$

In the case of a single orbiting electron, we can express the magnetic moment in terms of the electron charge $-e$ and its orbit radius r as follows:

$$\mu = IA = -\frac{ev}{2\pi r}\pi r^2 = -\frac{evr}{2},$$

where v is the velocity of the electron. Re-expressing this in terms of the angular momentum $L = mvr$ we end up with

$$\mu = -\frac{e}{2m}L.$$

If we choose $\vec{B}$ to be in the z-direction, only the z-component of the magnetic moment will be relevant, which is proportional to the z-component of the angular momentum $\vec{L}$. Recall that $L_z = \hbar m_l$. Using this in equation 2:

$$U = -\mu_z B = m_l \frac{e\hbar}{2m} B \tag{3}$$

where $\frac{e\hbar}{2m} =: \mu_B$ is called the Bohr magneton. We see that the energy levels are split for the different possible $m_l = -l, ..., +l$.

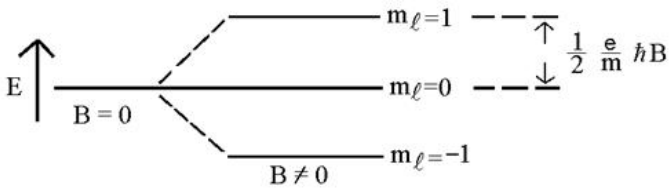

Figure 3: Zeeman splitting of the energy levels in the case of $l = 1$.

2.3 Dia- and Paramagnetism

The magnetisation M of a material is defined as the magnetic moment per unit volume. The magnetix susceptibility is a measure of how the magnetisation is dependent on the applied field:

$$\chi = \frac{M}{B}.$$

Diamagnetic substances have negative magnetic susceptibility, whilst paramagnetic substances have positive. The susceptibility is a cumulative effect due to effects at atom level. The atoms have three principle sources of magnetic moment: their spin, their orbital angular momentum and the change in moment due to an external applied field. The first two sources have diamagnetic effects. Their diamagnetic effect is similar to that of a coil producing a current to shield its interior against an applied field. The third source has a paramagnetic effect. [2]

The paramagnetic properties can be treated quantum mechanically. We discuss the magnetic moments of atoms and how they interact with a field. Similar to what we saw in the secion about the Zeeman effect, the magnetic moment of an atom (in free space) is given by

$$\vec{\mu} = -g\mu_B \vec{J}, \tag{4}$$

where μ_B is the Bohr magneton, $\vec{J}$ is the sum of $\vec{S}$ and $\vec{L}$ and g is called the **g factor**. The g factor for electrons is given by the Landé equation

$$g = 1 + \frac{J(J+1) + S(S+1) - L(L+1)}{2J(J+1)}. \tag{5}$$

In a magnetic field, this magnetic moment will generate potential energy given by

$$U = -\vec{\mu} \cdot \vec{B} = m_j g \mu_B B \tag{6}$$

and we recover the Zeeman effect but now for total magnetic moment $\vec{J}$.

2.4 Electron Spin Resonance

2.4.1 Absorption and g-factor

As seen in the previous section, the electron energy levels split in the presence of a magnetic field . Electrons can be excited between these levels by absorbing photons if the photon energy is equal to the energy gap:

$$\hbar\omega = g\mu_B B. \tag{7}$$

In ESR spectroscopy, the frequency of the incident photons and the size of the magnetic field can be tuned so that information about g can be obtained. In isotropic systems, g is a scalar, however in non isotropic systems it is a tensor so that the absorption energy gap is dependent on the incident direction of the photons. Without loss of generality, the g tensor can be diagonalised and has, depending on the symmetry of the system, maximally 3 degrees of freedom. [4]

The material investigated in this experiment, $CuSO_4{\cdot}5H_2O$, is symmetric in its z-axis. This means the g-tensor only has two independent components, $g_\perp$ and $g_\parallel$. They correspond to the values of g for light entering perpendicular or parallel to the symmetry axis, respectively. The g-tensor as a function of the incident angle to the symmetry axis is, by simple geometrical arguments, given by [5]

$$g = (g_\perp^2 \sin^2\theta + g_\parallel^2 \cos^2\theta)^{1/2}. \tag{8}$$

This equation allows us to recover $g_\perp$ and $g_\parallel$ from measurements of g at different angles.

2.4.2 Absorption spectrum and line broadening

In the experiment, the photons come from a radioactive source and have a constant frequency. By varying the applied field, an absorption graph can be made where there should be a peak at where the resonance condition 7 is fulfilled; at $B = \frac{\hbar\omega}{g\mu_B}$.

The peak is broadened due to several effects. The primary cause is the Heisenberg uncertainty relation: $\Delta E \Delta t = \frac{\hbar}{4\pi}$, where Δt is the relaxation rate of the exited electrons. This effect results in a Lorentz like resonance curve. Dipole-dipole interactions where a local field disturbance is dependent on the distance and orientation of neighboring spins can lead to Gauss or Lorentz like changes. Finally, exchange interactions are important in paramagnetic substances above a certain concentration of spins. The interactions force neighbouring spins to align and will make the curve less broad and more Lorentz like. [6]

In our experiment, we assume all these effects can play a role so the data is fitted to both Lorentz and Gauss curves.

2.5 Coppersulfate-Pentahydrate $CuSO_4{\cdot}H_2O$

The substance investigated in this experiment is $CuSO_4{\cdot}H_2O$ in both crystal and powder form. The unit cell of the crystal is depicted in figure 4.

The Cu^{2+} ions are surrounded by an elongated ocahedron with oxygen ions at the corners. This results in a tetragonal symmetry. This tetragonal symmetry has an effect on the g-tensor of the Cu^{2+} ions, namely that it only has two degrees of freedom which we call $g_\parallel$ and $g_\perp$.

The anisotropic surroundings of the Cu^{2+} ions also have an effect on the energy levels. Recalling figure 2, the five d-orbitals are split into a threefold degenerate t_{2g} orbital and a twofold degenerate e_g orbital. The t_{2g} orbitals are energetically more favourable in this configuration. [6]

3 Experimental setup

A ESR spectrometer is used consisting of the following parts (see figure 5):

1. Watercooled electromagnet with generator. Generates fields between 0 and 6 kG.

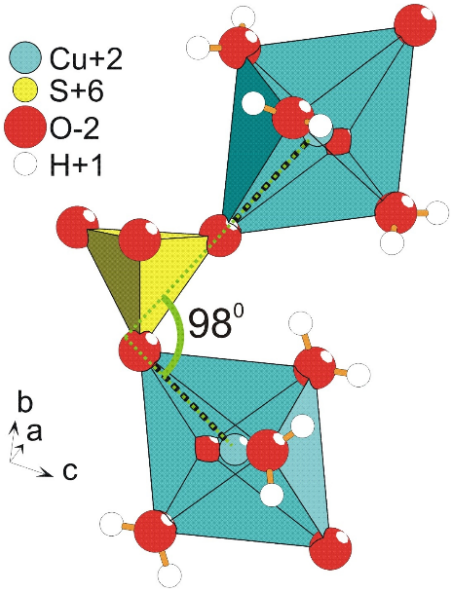

Figure 4: The unit cell of a $CuSO_4 \cdot H_2O$ crystal.

2. Microwave equipment: Klystron, microwave bridge, resonator, and detector
3. Data amplifier and recording

The sample is placed in the resonator. It absorbs the radiation from the klystron if the resonance conditions are fulfilled. The energy loss of the signal is detected as a voltage. During the experiment, the frequency of the radiation (about 10 GHz) is kept constant and the field is scanned, because it is easier to control the field in a precise way than it would be to control the radiation frequency. The field strength is measured with a Hall probe, attached directly between the magnetic poles, throughout the experiment. This way, the energy loss is registered as a function of the applied field.

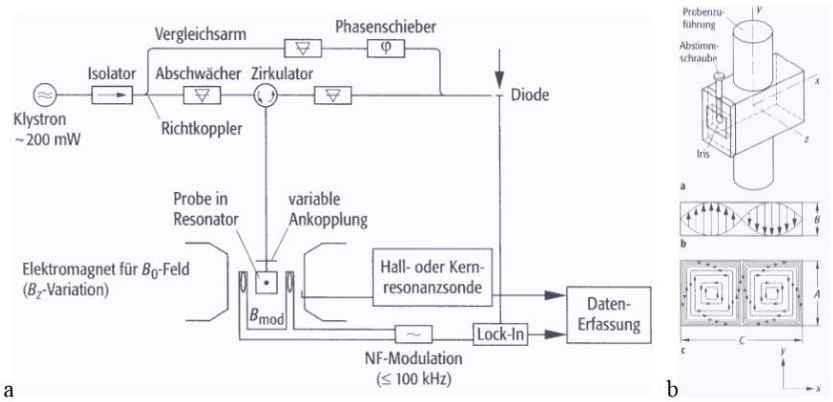

Figure 5: (a) The experimental setup of an ESR spectrometer. (b) The resonance cavity and the distribution of the standing electromagnetic wave inside.

Without processing, the detection signal would be too weak to be distinguishable from the background noise. This is solved by using a 'lock in' amplifier. It works by modulating the applied field with a small AC field. The sample reacts to this modulated field and the signal becomes sinusoidal. The amplitude of the signal change corresponds to the variation of absorbed energy in the resonator cavity. Now, the signal is of AC type and can be "filtered out" by the Lock-in amplifier and enlarged enough to be well separated from the noise, since the phase and frequency of the signal is known. Instead of an absorption signal, the recorded data are now the derivation from the absorption, see figure 6.

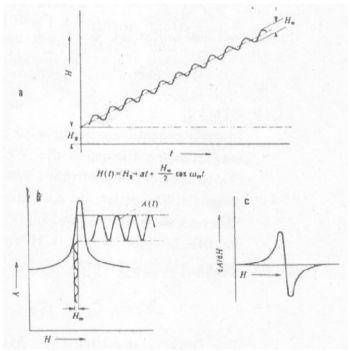

Figure 6: (a) The modulation of the external magnetic field. (b) Its influence on the resonance curve. (c) The ultimately detected signal: the derivative of the resonance curve.

4 Results

4.1 Single crystal measurements

In the first part of our experiments, we obtained resonance curves of a single crystal of $CuSO_4 \cdot 5H_2O$ in an external magnetic field, as a function of angle between the external field and crystalline axis (all angles between 0° and 180° with a step of 10°). For each angle, the external field was slowly varied between 2000 Gs to 4000 Gs, each time with the same field direction in order to eliminate possible hysteresis effect. The frequency of the incident microwave radiation was $\nu = 9.481 \pm 0.001$ GHz throughout all measurements. All obtained data can be found in the supplementary information of our report.

Let us briefly discuss the general properties of obtained data. As can be seen from the supplementary graphs, even though in theory the derivative of the resonance curve should be point-symmetric, it is not exactly the case for the obtained data. Furthermore, there is some background, which contributes to an offset in each graph. While analysing the data, this background was subtracted (in the supplementary graphs, this was already done).

Resonance curves should have either a Lorentzian or Gauss curve form [6]:

$$\text{Lorentz function: } I(B) = \frac{1}{\pi\gamma}\frac{\gamma^2}{((B-B_0)^2+\gamma^2)^2} \tag{9}$$

$$\text{Gauss function: } I(B) = \frac{1}{\sqrt{2\pi\sigma^2}}\exp\left(-\frac{(B-B_0)^2}{2\sigma^2}\right). \tag{10}$$

However, we measured not the absorbance itself, but its derivative. Therefore, the fitting functions were:

$$\text{for Lorentzian fit: } I'(B) = -I_0\frac{2\gamma}{\pi}\frac{(B-B_0)}{((B-B_0)^2+\gamma^2)^2} \tag{11}$$

$$\text{for Gaussian fit: } I'(B) = -I_0\frac{(B-B_0)}{\sqrt{2\pi\sigma^2}\sigma^2}\exp\left(-\frac{(B-B_0)^2}{2\sigma^2}\right) \tag{12}$$

.

In each case, I_0 and B_0 were fit parameters. The fits were made using Mathematica. B_0 corresponds to the magnetic field at which (maximum) absorbance takes place, I_0 is a scaling parameter and γ,σ are connected to full-width-at-half-maximum (FWHM) through relations:

$$\text{Lorentzian function: } FWHM = 2\gamma \tag{13}$$

Gaussian function: $FWHM = 2\sqrt{\ln 2}\sigma$. (14)

The obtained parameters with errors for Lorentzian and Gaussian fit functions are presented in Table 1 and Table 2, respectively. As can be seen from Fig.(11) in the supplementary information section, the resonance curve data for 10° and 20° does not differ significantly from the background and this leads to a large error. Therefore, these measurements were discarded.

θ in °	B_0 in Gs	ΔB_0 in Gs	FWHM in Gs	Δ FWHM in Gs
30	-2964.2	0.9	207.6	3.7
40	-2985.6	1.1	205.7	4.3
50	-3013.3	1.2	199.5	4.8
60	-3054.1	1.0	196.6	3.9
70	-3080	1.2	178	4.6
80	-3099.8	1.4	159.8	5.8
90	-3105.61	1.5	151	5.9
100	-3099.77	1.5	157.1	6.1
110	-3086.12	1.5	167.4	6.1
120	-3059.38	1.4	191.5	5.77
130	-3026.93	1.2	210.1	5.1
140	-3004.96	1	223	4.02
150	-2979.74	0.8	221.6	3.3
160	-2957.73	0.9	233.5	3.7
170	-2945.03	1.5	172.8	2.9
180	-2945.2	0.6	228.9	2.5

Table 1: Obtained parameters from the Lorentz fit

θ in °	B_0 in Gs	ΔB_0 in Gs	FWHM in Gs	Δ FWHM in Gs
30	-2963.7	1.2	124.5	2.0
40	-2984.8	1.2	125.3	2.0
50	-3012	1.2	121.9	2.1
60	-3053.23	1.1	118.4	1.8
70	-3080	1.2	104.9	2.0
80	-3101.3	1.3	92.4	2.1
90	-3107.6	1.2	87.8	1.9
100	-3101.8	1.3	90.7	2.1
110	-3087.3	1.4	97.6	2.4
120	-3058	1.5	117	2.5
130	-3025.2	1.3	129.7	2.3
140	-3004.2	1.2	138	2.0
150	-2980.29	1.1	136.1	1.8
160	-2957.7	1.2	144.3	2
170	-2945	1.5	143.9	2.5
180	-2944.5	1.2	138	2.1

Table 2: Obtained parameters from the Gauss fit

Furthermore, the g-factor was determined for each angle and for both fits using the resonance condition 7:

$$g(\theta) = \frac{h\nu}{\mu_B B_0(\theta)} \tag{15}$$

All obtained results are shown in Table 3.

A graph of the dependence of the g-factor on the angle is shown in Fig.(7). The points were fitted using the theoretically derived formula 8 in order to obtain $g_\perp$ and $g_\parallel$ (Table 4):

$$g = \sqrt{g_\perp^2 \sin^2\theta + g_\parallel^2 \cos^2\theta} \tag{16}$$

θ in °	g-factor, Lorentz fit	g-factor, Gauss fit
30	2.285	2.286
40	2.269	2.270
50	2.248	2.249
60	2.218	2.219
70	2.199	2.199
80	2.185	2.184
90	2.181	2.180
100	2.185	2.184
110	2.195	2.194
120	2.214	2.215
130	2.238	2.239
140	2.254	2.255
150	2.273	2.273
160	2.290	2.290
170	2.300	2.300
180	2.300	2.301

Table 3: The obtained g-factors from Lorentzian and Gaussian fits

	Lorentz fit	Gauss fit
$g_\perp$	2.1838	2.1834
$g_\parallel$	2.3085	2.3092

Table 4: $g_\perp$ and $g_\parallel$ from Lorentz and Gauss fits.

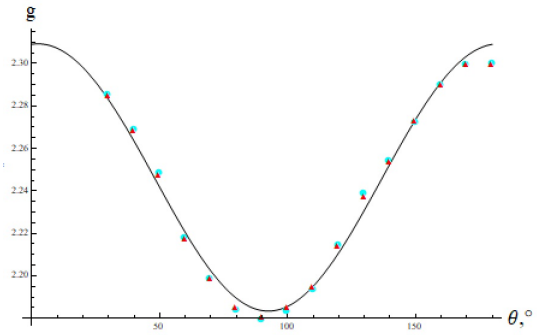

Figure 7: Dependence of g-factors on angle from Lorentz (red triangles) and Gauss fit (cyan dots) with fitting function.

As can be seen, the obtained values for the g-factors are very similar for the Lorentzian and Gaussian fits.

Fitting errors were determined by mathematica. The measurement errors were determined using

$$\Delta g(\theta) = \frac{h\nu}{\mu_B B_0(\theta)} \sqrt{\left(\frac{\Delta\nu}{\nu}\right)^2 + \left(\frac{\Delta B_0(\theta)}{B_0(\theta)}\right)^2}. \tag{17}$$

The obtained values lie in interval of $\Delta g = (0.0007...0.0011)$ and are very small in comparison to the obtained g-factors. Line broadening could have had a big contribution to the errors but we did not include it in our analysis.

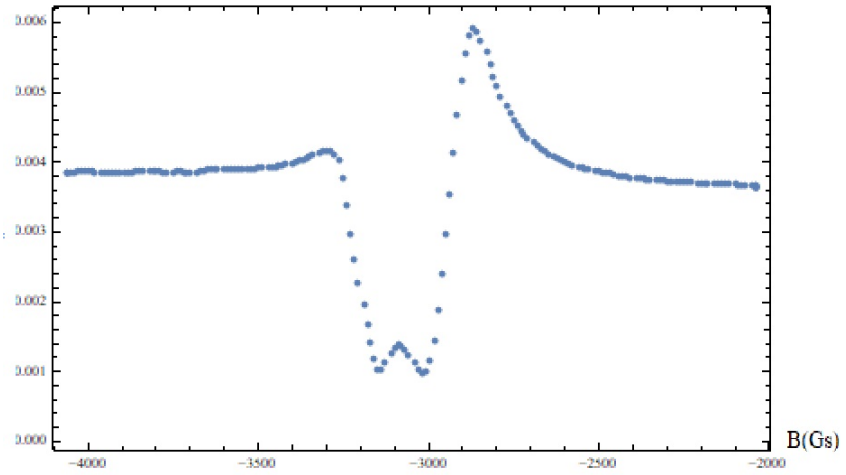

Figure 8: Resonance curve for powder sample

4.2 Powder

The next part of our experiment was measuring the resonance curve for a powder sample of $CuSO_4{\cdot}5H_2O$. It is necessary to make only one measurement, as powder already consists of crystals of all possible orientations between the crystalline axis and the external magnetic field. The obtained data is shown in Fig.(8).

We used the procedure described in [7] to obtain $g_\perp$ and $g_\parallel$. $g_\perp$ can be determined by plugging the field where the data shows a minimum into the resonance condition, $g_\parallel$ by plugging in the field at the maximum. We found the maximum at $B_{max} = -2870$ Gs and the minimum at $B_{min} = -3020$ Gs of the resonance curve. The error in the magnetic field was estimated as half the distance between the nearest points:

$$g_\perp = g(B_{min}) = 2.2430 \pm 0,0037$$
$$g_\parallel = g(B_{max}) = 2.3602 \pm 0,0041$$

The obtained values of g-factor are in the same order of magnitude as those which were found in the single-crystal and as presented in the paper by Kneubühl. [7].

5 Conclusion

$CuSO_4{\cdot}5H_2O$ was analysed both in single crystal form and powder form. ESR measurements were applied to study the absorption shapes and the angle dependence of the resonance. From this, we learned about the ESR techniques as well as the structure of $CuSO_4{\cdot}5H_2O$, especially its g-factor components.

From the single crystal measurements, we found:

	Lorentz fit	Gauss fit
$g_\perp$	2.1838	2.1834
$g_\parallel$	2.3085	2.3092

From the powder measurements:

$$g_\perp = g(B_{min}) = 2.2430 \pm 0,0037$$
$$g_\parallel = g(B_{max}) = 2.3602 \pm 0,0041.$$

The results agree with each other reasonably well. They are also roughly equal to the results presented in the papers by Kneubühl[1] and Wheatley&Halliday [5, 7]:

[1] In Kneubühls paper, $g_\parallel$ and $g_\perp$ might have been switched around by mistake.

	Kneubühl	Wheatley & Halliday
$g_\perp$	2.27	2.07
$g_\parallel$	2.08	2.39

Not all measurements were as clean and symmetrical as expected. To get better results, more attention could be given to the background noise and to fine-tuning the equipment. Furthermore, the line broadness could be investigated to learn more about internal coupling processes.

References

[1] F. Sears, M. Zemansky, H. Young, and R. Freedman, *University Physics with Modern Physics: Technology Update*, ch. 41: Atomic Structure. Pearson, 13 ed., 2014.

[2] C. Kittel, *Introduction to Solid State Physics*, ch. 11. Wiley, 8 ed., 2004.

[3] A. Biswas, K.-S. Kim, and Y. H. Jeong, "Metal-insulator transitions and non-fermi liquid behaviors in 5d perovskite iridates," *arXiv preprint arXiv:1508.04929*, 2015.

[4] B. M. Weckhuysen, R. Heidler, and R. A. Schoonheydt, "Electron spin resonance spectroscopy," in *Characterization I*, pp. 295–335, Springer, 2004.

[5] J. Wheatley and D. Halliday, "Paramagnetic absorption in single crystals of copper sulfate pentahydrate," *Physical Review*, vol. 75, no. 9, p. 1412, 1949.

[6] University of Cologne - Physics institute II, "Tutorial: Experiment m2.6, electron spin resonance."

[7] F.K.Kneubuehl, "Line shapes of esr signals produced by powders...," *J.Chem.Phys*, vol. 33, pp. 1074–1078, 1960.

6 Supplementary information

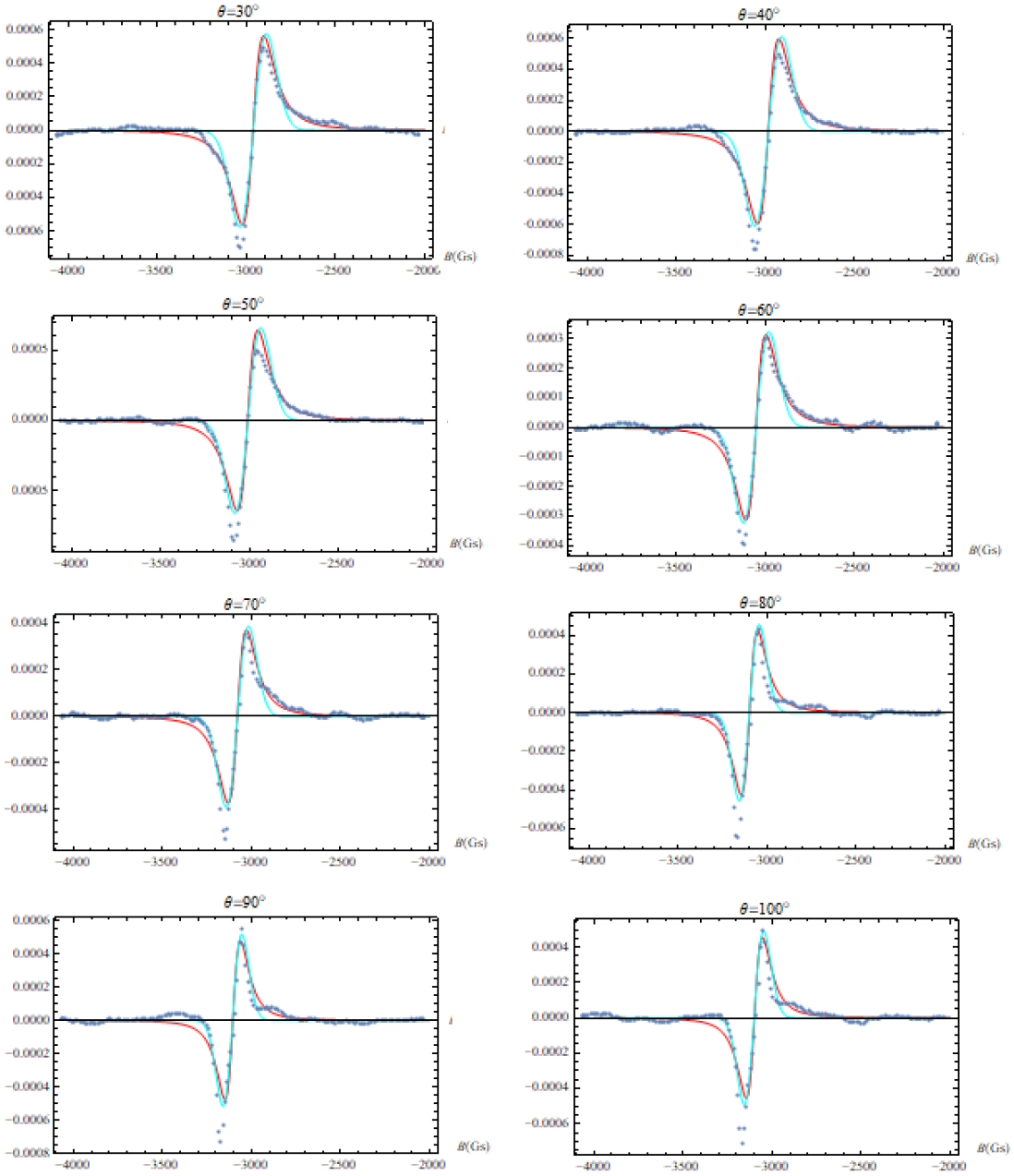

Figure 9: Obtained data for $\theta = 30° - 100°$ with subtracted background. Red and cyan lines denote Lorentzian and Gaussian fit, respectively. The y-axis is in relative units here.

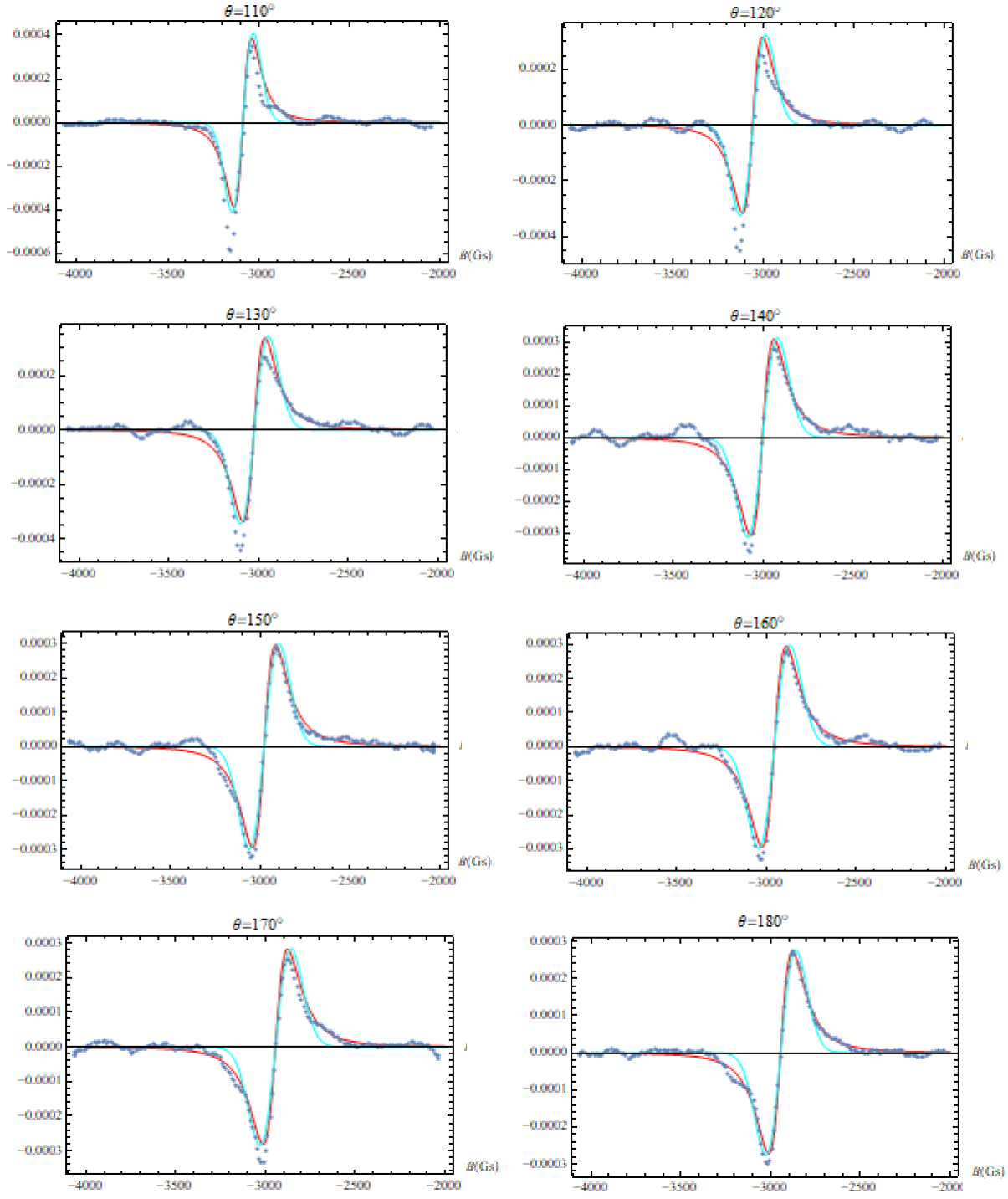

Figure 10: Obtained data for $\theta = 110° - 180°$ with subtracted background. Red and cyan lines denote Lorentzian and Gaussian fit, respectively.

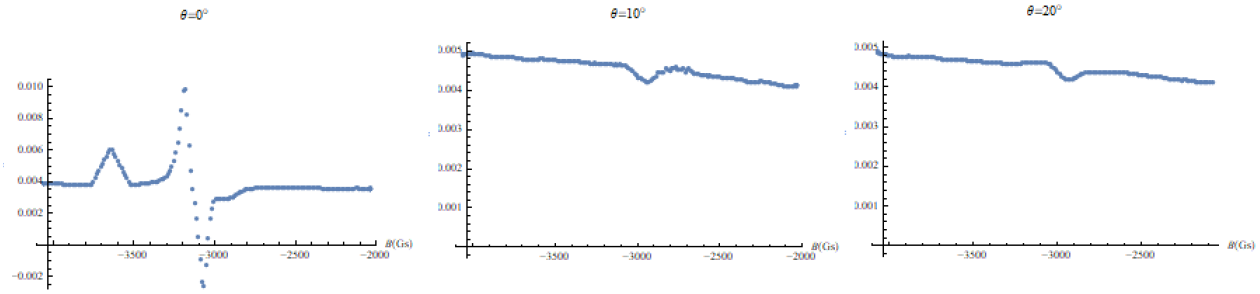

Figure 11: Obtained data for $\theta = 0° - 20°$
without subtraction of background.These measurements were discarded.